Capillarity and Dielectrophoresis of Liquid Deuterium

Introduction

The current target used for laser-driven inertial confinement fusion experiments is a shell (0.9 mm in diameter) with a 100-μm-thick wall of solid cryogenic deuterium and tritium (DT) ice.[1] The interior of this shell contains more DT, but in liquid form. Future more-powerful laser drivers, such as the National Ignition Facility constructed at Lawrence Livermore National Laboratory, will use larger targets—up to ~4.7 mm in diameter with ~350-μm wall thickness and yielding energies up to ~18 MJ each.[2] The present approach to making these targets is to create shells of a low-density polymer foam and then to use these as mandrels to form the final DT-ice structures. Using current techniques, these targets, which are very complex with stringent mechanical specifications, are batch produced in a process that takes as long as two weeks.[3] Given the sizeable tritium content for the larger targets (>15 Ci) and the fact that a fusion-powered electric power plant of reasonable size (~1000 MW) will consume >500,000 of these targets per day,[4] such a long production cycle would necessitate an exceptionally large inventory of highly radioactive tritium. To reduce these inventories to tractable levels, a fully automated, just-in-time approach to target production is needed. It is our proposition that a system based on microfluidics may be able to meet this requirement.[5]

One critical step in target preparation is the fueling process, where liquid DT is loaded into the shells, which themselves are fragile. The current technique involves permeating the gas through an outer membrane, a process requiring a slow pressure ramp-up to an ultimate value of 1000 bars.[6] For a commercial-scale fusion power plant, this process is far too slow and cumbersome. Furthermore, it necessitates a level of human intervention that is undesirable in any commercial process involving a highly mobile radioactive isotope such as tritium. Therefore, an important goal of the present program is to develop an alternate technique for fueling of laser targets. In this article, we report on experiments that use the dielectrophoretic (DEP) force to manipulate liquid deuterium remotely and reliably at temperatures below ~30 K. In the early years of the space program, liquid DEP was seriously considered as a means to manage cryo-propellants in zero gravity,[7,8] so it is only natural to reopen its consideration for the present application.

Background

Liquid DEP enlists the so-called ponderomotive force, which selectively attracts dielectric liquids with relatively higher dielectric constant into regions where the imposed electric field is stronger. Fluids with relatively lower dielectric constant, including vapor and gas, are simultaneously repelled from the strong electric field. The critical requirement for DEP liquid management is the nonuniformity of the electric field imposed by the particular design of the electrodes. The dielectrophoretic effect is influenced by the electrical conductivity (σ) of the liquid. In general, joule heating presents a serious obstacle to the use of liquid DEP management when $\sigma > \sim 10^{-4}$ S/m [which is the conductivity of deionized (DI) water]; but most liquid cryogens, including H_2 and D_2, are very highly insulating dielectrics. As a result, DEP manipulation of such liquids is relatively easy to exploit using properly designed electrodes and easy to control via voltage modulation.[a]

Despite obvious difficulties in handling them, the critical properties of the isotopes of cryogenic hydrogen—H_2, D_2, and T_2—have been intensively studied. Many published measurements as well as some crucial extrapolations intended to fill gaps in the data have been obtained.[9] We can anticipate that the microfluidic behavior of cryogenic liquid hydrogen will be unique based on its physical properties. For example, liquid deuterium has very low density (~0.18 gm/cm^3), dielectric constant ($\kappa \sim 1.25$), and surface tension (0.0038 N/m), at least compared to room-temperature liquids. Furthermore, the liquid maintains zero contact angle against almost all solid materials.[10] Also, the useable range of temperatures and (saturated vapor) pressures spans conditions from the triple point (T = 18.7 K, p = 17 kPa) almost to the critical point (T = 38 K, p = 1.7 MPa), the consequence being rather strong temperature

---

[a]Due to its radioactivity and abundant β particles, tritium may very well behave like a conductive liquid. Some speculation on the effect of such bulk charge transport on electric field–mediated microfluidics is considered in the **Discussion** section of this article.

dependencies for some of the important fluid properties. Low viscosity creates still another distinction of likely importance in the dynamics of target fueling, although this issue is not addressed in this article. For ~10 to ~100-μl-D_2 droplets (the size range appropriate for laser targets), the capillary force is significant, but the liquid DEP force can be made comparable or dominant if care is taken to avoid electric breakdown.

This article presents experiments with a simple, parallel plate geometry intended to investigate the basic capillary and DEP force-coupled hydrostatics of liquid D_2 in the temperature range from ~19 to ~27 K. We find that a simple model adequately describes the effectively additive natures of the capillary and DEP forces upon the net height of rise against gravity. We further demonstrate a hydrostatic bifurcation effect that might ultimately be exploited in dispensing and metering liquid D_2 for application in the fueling of laser targets.

Basic Theory

The capillary rise of a liquid covered by a gas or vapor of negligible density between two parallel and vertical plates is h_{cap} (Ref. 11):

$$h_{cap} \approx 2\gamma \cos\theta_c \big/ (\rho_1 - \rho_v)gd, \tag{1}$$

where γ = surface tension, ρ_1 and ρ_v = liquid and vapor mass densities, θ_c = contact angle, d = plate spacing, and $g = 9.81$ m/s^2 is the terrestrial acceleration caused by gravity. Usually, $\rho_1 \gg \rho_v$. The geometry is illustrated in Fig. 118.37(a). Equation (1) assumes that $h_{cap} \gg d$ and also that the plates

are wide compared to their spacing, that is, $w \gg d$. The Bond number (Bo), a useful dimensionless modulus that may be identified from Eq. (1),

$$\mathrm{Bo} \equiv h_{cap}\big/d = 2\gamma \cos\theta_c \big/ (\rho_1 - \rho_v)gd^2 \tag{2}$$

measures the relative importance of surface tension and gravity. For Bo $\gg 1$, the transverse profile of the liquid meniscus between the plates assumes the shape of a circular arc. In the classic case of a sessile droplet resting on a flat surface, one replaces the plate spacing d in Eq. (1) by the droplet radius. Then, the magnitude of Bo tells us whether the droplet takes the shape of a spherical cap (Bo $\gg 1$) or a flattened disk (Bo $\ll 1$).

If the liquid is a dielectric, the plates are conductive electrodes, and voltage V is applied between them, the ponderomotive (DEP) effect exerts an additional upward force on the liquid column [refer again to Fig. 118.37(a)]. Pellat studied this behavior in 1895.[12] Assuming, as before, that the plates are very wide compared to the spacing, the dielectric height of rise is[13]

$$h_{DEP} \approx (\kappa_1 - \kappa_v)\varepsilon_0 V^2 \big/ 2(\rho_1 - \rho_v)gd^2, \tag{3}$$

where κ_1 and κ_v are the liquid and vapor dielectric constants, respectively, $\varepsilon_0 = 8.854 \times 10^{-12}$ F/m, and V is the rms voltage applied to the electrodes. Note that typically $\kappa_v \approx 1.00$. It is convenient here to define a new dimensionless modulus called the electric Bond number (Be):

$$\mathrm{Be} \equiv h_{DEP}\big/d = (\kappa_1 - \kappa_v)\varepsilon_0 V^2 \big/ 2(\rho_1 - \rho_v)gd^3. \tag{4}$$
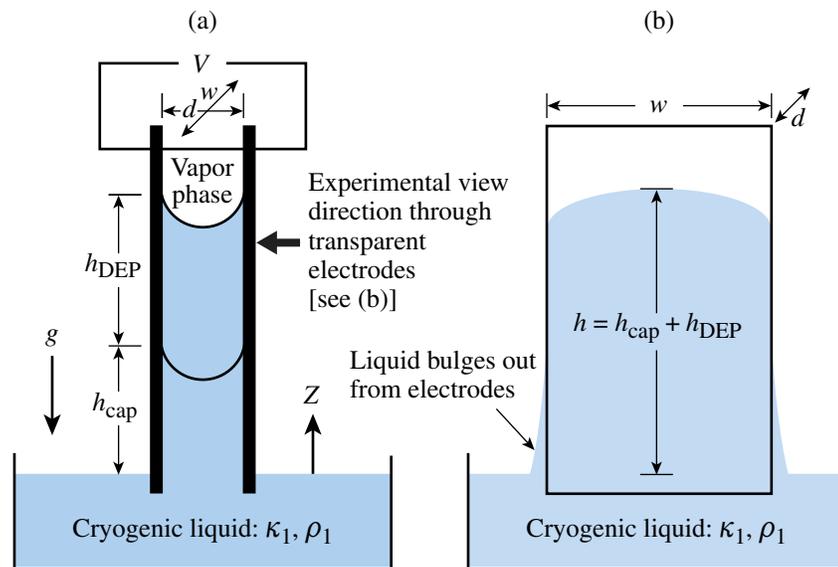
Figure 118.37
The parallel plate geometry. In the absence of voltage, the capillary rise is h_{cap}. (a) The side view depicts the expected circular profile of the meniscus and the contact angle $\theta_c = 0°$, which characterizes deuterium with almost all solids. When voltage is applied, the liquid rises an additional amount h_{DEP}. Unlike electro-wetting, the DEP force has virtually no influence on the contact angle. (b) Cross sections show the liquid bulging outward toward the bottom.

E18027JR

This modulus measures the strength of the DEP force compared to gravity.

Note that Eqs. (1) and (3) are additive contributions to the *hydrostatic* equilibrium; neither capillarity nor DEP can develop the dynamic pressure head required to pump liquid continuously from point to point. If a temperature gradient is properly imposed along the length of an electrode structure, as in the case of the dielectrophoretic heat pipe,[14] liquid motion can be induced, but it is the temperature gradient that drives the motion, not the electric field. No time-average electric power is supplied to the system, just as the wick in a capillary heat pipe supplies no pumping power. It is also possible to siphon dielectric liquid between an upper and a lower reservoir using the DEP effect.[15] The electric field imposed by the electrodes maintains fluid communication between the reservoirs but, just as in a regular tube siphon, gravity establishes the pressure head that moves the liquid.

Elementary considerations reveal that the capillary and DEP contributions to the height of rise are simply additive, so that the net measurable effect is $h = h_{cap} + h_{DEP}$. The ratio Be/Bo measures the relative importance of the DEP and capillary contributions:

$$\frac{Be}{Bo} = \left(\kappa_1 - \kappa_v\right)\varepsilon_0 E^2 d \Big/ 4\gamma \cos\theta_c , \qquad (5)$$

where the rms (root-mean-square) electric field strength $E = V/d$ appears in Eq. (5). Electrical breakdown in the covering gas or vapor usually imposes a limit on the maximum electric field, that is, $E < E_b$. For saturated D_2 vapor at $T = 20$ K, the breakdown field strength is $E_b \approx 2 \times 10^7$ V_{rms}/m (Ref. 16). Equation (5) shows that, if the electric field E is limited by breakdown, the way to increase the relative importance of the DEP force is to increase κ, d, or θ_c. Assuming an electrode spacing of $d = 1$ mm, a safety margin for the applied electric field of $E = 0.25 \, E_b$, and using the properties of liquid D_2 at $T = 20$ K, Eq. (5) gives Be/Bo ≈ 3.5. As a result, the DEP force can be made to dominate over capillary rise.

The hydrostatic profile of the liquid along the vertical sides is difficult to model because it depends on hard-to-determine details of the shape of the sides of the plates. The vertical profile is further influenced by the strongly nonuniform electric field. In general, the liquid always bulges outward near the bottom and recedes inward near the top, as depicted with some exaggeration in Fig. 118.37(b). For cryogenic deuterium, with its low surface tension $\gamma \approx 0.0038$ Nt/m and zero contact angle $\theta_c \approx 0°$, this bulging is actually minimal. The highest reach of the liquid occurs midway between the edges of the electrodes. On either side of the high point, the meniscus curves steadily down to where it becomes vertical along both edges. The 3-D shape of the liquid surface at the top of the column is best predicted by numerical means.

Experiments Using Parallel Electrodes

The experimental plates are made of glass treated with indium tin oxide (ITO), 1.1 mm thick, ~15 mm high, and 7.6 mm wide. The ITO layer is conductive but transparent, making it possible to observe and record the shape of the liquid meniscus along the width of the electrodes. The electrode assembly is placed in a chamber connected to a cryostat so that it can be cooled as low as the triple point of D_2. By carefully managing the inventory of gaseous deuterium introduced into the cryostat and controlling the temperature, we condense liquid D_2 in a pool at the bottom of the chamber. This pool serves as the reservoir depicted in Figs. 118.37(a) and 118.37(b). The viewing ports in the present experimental chamber are on the top and bottom, requiring placement of a mirror inside to view the liquid rise.

Figure 118.38 shows the liquid rise viewed through the ITO-treated glass electrodes for a range of applied voltages. It is important to note that the profile of the meniscus along the width of the electrodes does not change appreciably as the voltage is increased, indicating that the electric field has negligible influence on the curvature of the liquid/vapor surface. Height-of-rise data from individual digital images like those in Fig. 118.38 are gathered by measuring the vertical distance from the equilibrium level of the liquid in the pool to the highest point of the meniscus. Despite small systematic errors, due primarily to uncertainty about the exact location of the equilibrium liquid level outside the plates, these data compare quite favorably to the 1-D model prediction. Figure 118.39(a) plots the net height-of-rise data for experiments performed at several temperatures. The solid lines in this figure are predictions for $h = h_{cap} + h_{DEP}$ based on the 1-D hydrostatic models used to obtain Eqs. (1) and (3). For these curves, we employed the set of approximate, fitted temperature-dependent expressions for dielectric constant $\kappa_1(T)$, liquid and vapor densities $\rho_1(T)$ and $\rho_v(T)$, and surface tension $\gamma(T)$ found in the **Appendix**. Some of the data are obtained at temperatures lying outside the advertised range for the dielectric constant expression, but any resulting error is not expected to be significant because $\kappa_1(T)$ is a rather weak function of temperature.

Figure 118.39(b) plots measured height-of-rise data and predictive curves directly as a function of temperature T for several fixed voltage values. While voltage—actually the electric
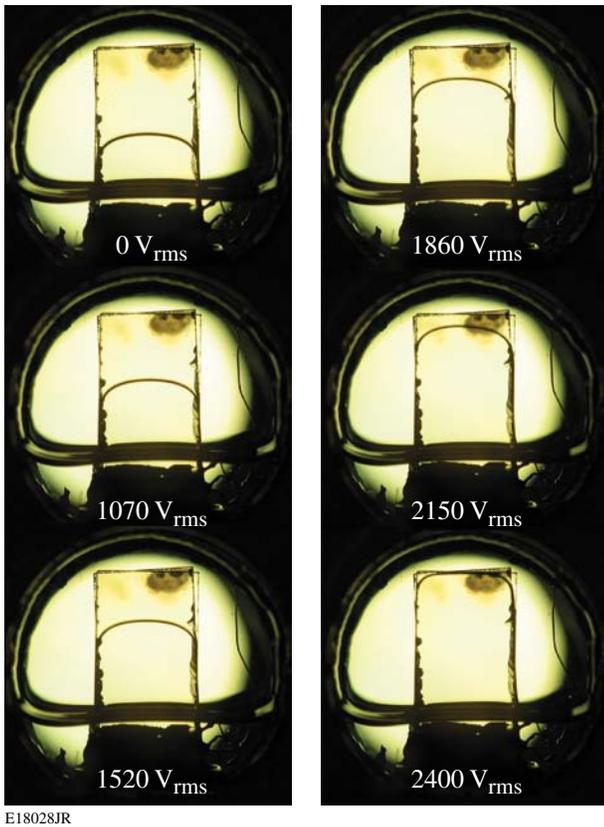
Figure 118.38

Meniscus of cryogenic D_2 at $T = 18.7$ K viewed through parallel, transparent ITO glass electrodes; $w = 7.6$ mm, $d = 0.86$ μm for 1-kHz ac voltages ranging from 0 to 2400 V_{rms}. Frequency must be high enough to avoid surface wave instabilities but is otherwise not important.

field magnitude $E = V/d$—does not influence the shape of the meniscus, the images in Fig. 118.40 do reveal that the temperature does have some effect. The measured radius of curvature in the plane of the electrodes at the midpoint increases from ~7 mm at $T = 18.8$ K to ~11 mm at $T = 26.9$ K, reflecting an ~45% drop in the surface tension at the higher temperature. Over this same temperature range, the density changes by only ~10%. Temperature is not believed to appreciably influence the contact angle θ_c.

One factor very critical to the success of Eqs. (1) and (3) in predicting the net height of rise is the condition $w \gg d$, where w and d are, respectively, the plate width and spacing. In this limit, the influence of the vertical sidewalls becomes less and less significant, and the uniform electric field approximation inherent in Eq. (3) becomes more valid. A 1-D model, of course, cannot predict the curved profile evident in the images of Fig. 118.38. To overcome this modeling deficiency, a finite-element computation was used to solve for the 3-D surface
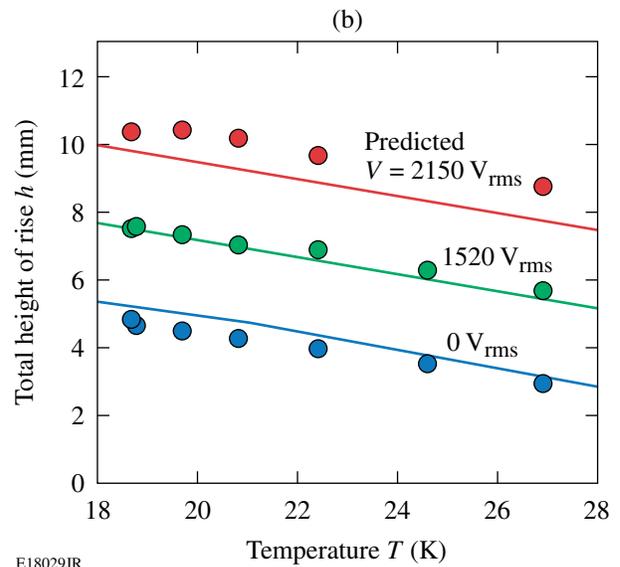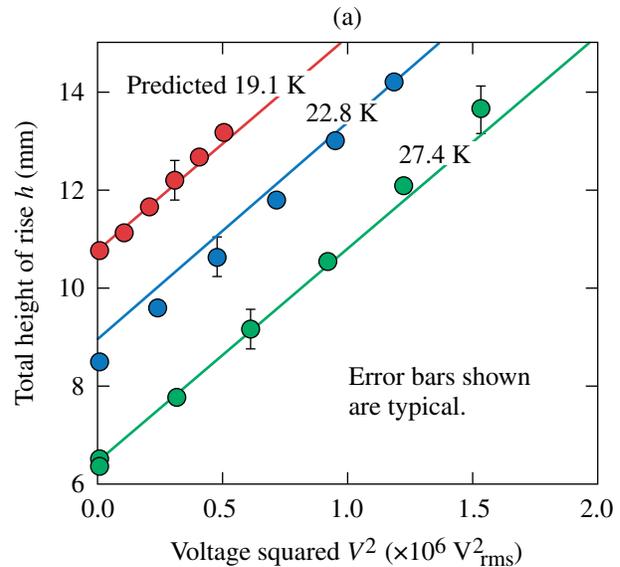
Figure 118.39

Height-of-rise data and predictions using $h(V) = h_{cap} + h_{DEP}(V)$ for liquid deuterium using parallel electrodes: $w = 7.6$ mm, $d = 0.43$ (±0.02) mm. (a) h versus voltage V at various temperatures; (b) h versus temperature at several fixed voltages.

between the plates. This analysis, based on a numerical energy minimization, is summarized in the next section.

Simulations

The significant curvature of the liquid surface parallel to the electrode plates evident in Fig. 118.38 reveals that surface wetting can influence the maximum, measurable height of rise, h, if the plates are not sufficiently wide. For this reason, we used the Surface Evolver software of K. Brakke[17] to solve for the

18.8 K, 0 V
Radius of curvature ≈ 7.3 mm
Measured at midpoint

26.9 K, 0 V
Radius of curvature ≈ 11.0 mm
Measured at midpoint

E18030JR
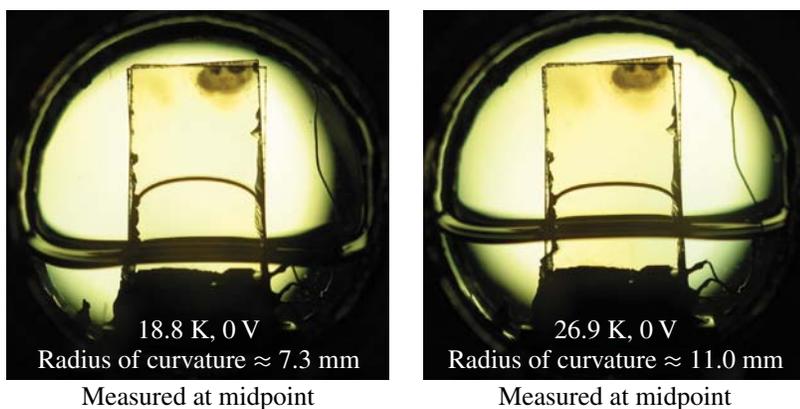
Figure 118.40
Effect of temperature on meniscus shape. The tempera-ture, but not the electric field E, influences the profile of the meniscus along the width of the electrodes through its influence on surface tension and density.

shape of the liquid meniscus. This finite-element tool is based on a computational algorithm that seeks the minimum energy configuration of a static liquid volume subject to wall con-straints, contact angle, gravity, and certain other body forces.[b]

Figure 118.41 shows various views of the numerical solution for the meniscus of D_2 using geometric parameters representa-tive of the actual experiment, at temperature $T = 18.7$ K and with no voltage applied. Figure 118.41(a) provides an oblique view of the elevated liquid between the plates, and Fig. 118.41(b) shows an end-on view of the meniscus. One thing to note about the numerical solution is that the contact angle made by the liquid at the walls does not quite go to zero, presumably because of the level of mesh refinement. An enlarged view of the meniscus, shown in Fig. 118.41(c), reveals details of the actual 3-D liquid surface near the top. Note that the two radii of curvature are of opposite signs. It is for this reason that the liquid height at the midpoint is always less than the value pre-dicted by the 1-D model. The view normal to the parallel plates [Fig. 118.41(d)] is the same afforded by viewing the experiment through the transparent ITO glass plates. A curve fitted to an experimental image of the actual meniscus is superimposed for comparison. Correspondence is reasonable, except for very close to the vertical edges of the plates, where the actual loca-tion and configuration of the contact line cannot, in fact, be modeled with any confidence. The height of rise h_{cap} calculated from the 1-D model [Eq. (1)] is also provided in Fig. 118.41(d).

To investigate in greater detail the influence of plate width w on the profile of the liquid deuterium meniscus and the height of rise h_{cap}, additional simulations were performed using Surface Evolver. Again, the DEP effect was not incorporated into the model. These results, shown in side view only, are provided in Fig. 118.42. Note that as the width is increased, the maximum height of the meniscus at the midpoint approaches h_{cap}, which

(a) Oblique view   (b) End-on view

(c) Meniscus detail   (d) Side view

E18031JR
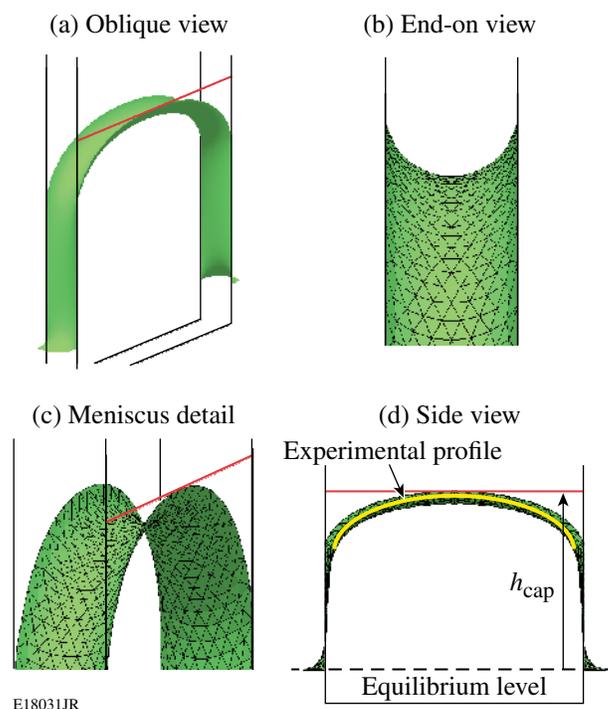
Figure 118.41
Numerical solution obtained using Surface Evolver software for the shape of the liquid meniscus between parallel plates for $w = 7.6$ mm, $d = 0.86$ mm, and $T = 18.7$ K. (a) Oblique view; (b) end-on view showing the contact angle $\theta_c \approx 0°$; (c) close-up of the meniscus; (d) view perpendicular to parallel plates with superimposed image from the experiment.

[b]The Surface Evolver software accommodates any body force that can be trans-formed into a surface or line force using the divergence theorem. In principle, electrical forces can be handled in this fashion; however, solution for the electric field on each facet of the mesh becomes necessary. Convergence then involves solving a tightly coupled problem where the mesh and the highly nonuniform electric field influence one another, i.e., both electric field and surface shape must be solved simultaneously. Surface Evolver is not designed to do this.

is predicted by the 1-D model [i.e., Eq. (1)]. For the value of the plate spacing used in the calculation, $d = 0.86$ mm, this point is reached at $w \approx 7$ mm. For larger values of w, the meniscus exhibits a virtually flat section in the middle. It is evident, both from experiment and from the simulations supporting them, that the vertical sidewalls' influence on the profile can be significant.

Experiments Using Converging Electrodes

The electrohydrostatic behavior of dielectric liquids becomes more interesting if the electrodes, still planar, are made to converge toward the top, as shown in Fig. 118.43(a). If the ratio of the spacing at the bottom and the top, b/a, is large enough, the liquid column exhibits a bifurcation, which was first observed with conventional room-temperature dielectric liquids. If the electrodes are planar, the relationship of the height of rise h to the applied voltage V takes the form of a cubic equation whenever $a \neq b$. This equation is obtained using the Maxwell stress tensor and hydrostatic pressure balance to account for the upward DEP force, under the assumption $a < b \ll w < H$:

$$\underline{h}^3 - 2\underline{h}^2 + (1 + \text{Bo})\underline{h} - (\text{Bo} + \text{Be}) = 0, \qquad (6)$$

where $\underline{h} = \alpha h/b$ is the normalized height of rise, a and b are the plate spacings at the top and bottom, respectively, H is the electrode height, and $\alpha = (b-a)/H$. A derivation of Eq. (6) is presented elsewhere.[18] If $a < b \ll H$, then α is approximately the angle between the plates in radians. For convenience, Eq. (6) employs modified definitions for the Bond numbers given below:

$$\text{Bo} = 2\alpha\gamma\cos\theta \big/ (\rho_1 - \rho_v) g b^2$$

$$\text{and} \qquad (7)$$

$$\text{Be} = \alpha(\kappa_1 - \kappa_v)\varepsilon_0 V^2 \big/ (\rho_1 - \rho_v) g b^3.$$

5 mm   6 mm   7 mm   8 mm

h_{cap}

E18032JR
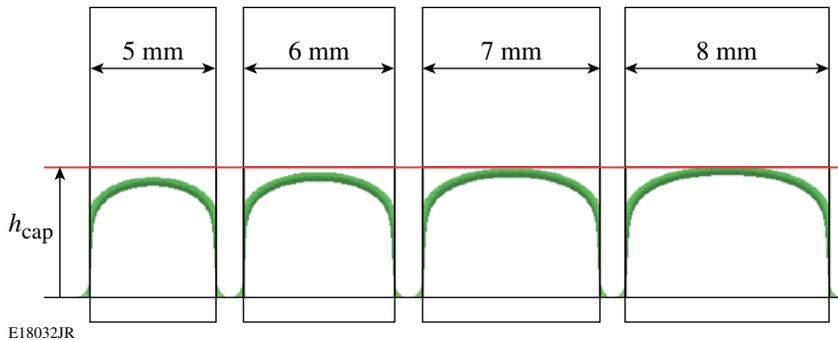
Figure 118.42
Side view of liquid D_2 meniscus profile between plates of spacing $d = 0.86$ mm at $T = 18.7$ K calculated using Surface Evolver for different values of the plate width: $w = 5, 6, 7$, and 8 mm. The top of the liquid column does not reach h_{cap}, the value predicted by the 1-D model, unless $w \geq 7$ mm. This result certainly scales directly with plate spacing d.

(a)

V
a
H
h
b
Z

Experimental view direction through transparent electrodes

(b)

$h(V)$

Top of electrodes
H
Unstable
h^* Bifurcation point
Stable
V^* V

E18033JR
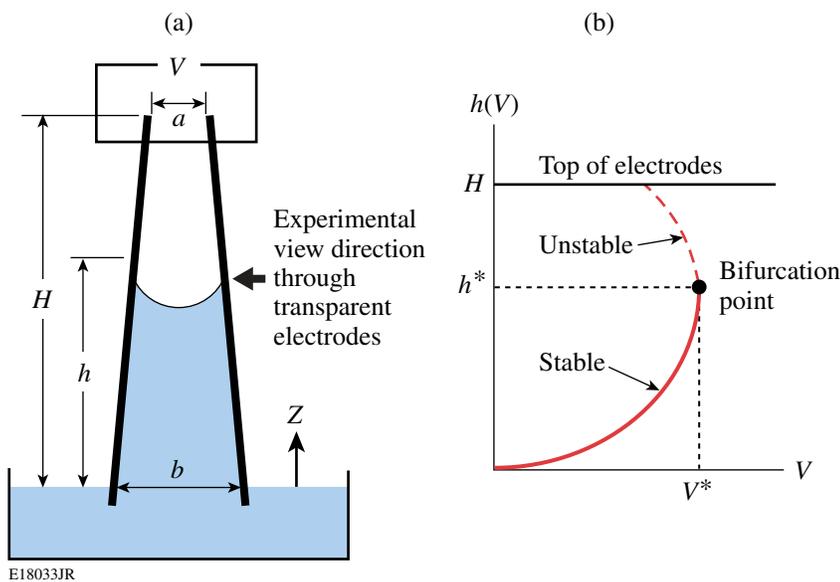
Figure 118.43
The converging plate experiment. (a) Electrode geometry and definitions of parameters. (b) Representative $h(V)$ curve with bifurcation point at (V^*, h^*). A bifurcation of the hydrostatic equilibrium is expected only if the electrode height H exceeds the critical value, i.e., $H > h^*$.

Given the cubic nature of Eq. (6), the easiest way to explore the hydrostatics of the converging plate geometry is to plot V as a function of $\underline{h}$. Referring to Fig. 118.43(b), the point on the curve where $dh/dV \longrightarrow \infty$, identified as (V^*, h^*), becomes an observable bifurcation of the hydrostatic equilibrium if the condition $0 < h^* < H$ is met. For this case, as voltage is increased, the liquid column rises steadily upward until, at voltage V^*, it jumps from $h = h^*$ all the way to the top of the electrodes, i.e., $h \longrightarrow H$. If the liquid column is already at the top and the voltage is turned back down, then, according to the model, static equilibrium is lost on both vertical sides at the same point, $z = h^*$, where the liquid jump occurred, and at the same voltage $V = V^*$. It is easily shown from pressure balance arguments that, as the voltage is being reduced, $z = h^*$ will always be the first point on the entire free surface where hydrostatic pressure equilibrium can no longer be maintained. The surface thus collapses inward on both sides at $z = h^*$, usually trapping liquid at the top. This trapped inventory remains near the top even when the voltage is reduced to zero, possibly because of contact angle hysteresis. While this behavior occurs just as predicted in the case of room-temperature dielectrics,[18] experiments using cryogenic D_2 yield some differences.

Figures 118.44 and 118.45, respectively, show images from an experiment performed using liquid deuterium with the voltage first monotonically increased and then decreased. For increasing voltage (Fig. 118.44), the column rises steadily until, at some voltage between 1590 and 1599 V_{rms}, it jumps the rest of the way to the top, just as predicted by the 1-D model. On the other hand, when the voltage is then reduced (Fig. 118.45), the surface does not fully collapse at $V = V^*$ but instead forms a neck that becomes narrower and narrower as V is further reduced. Eventually, the neck does rupture, but our observation is that the volume of liquid trapped near the top is neither well controlled nor very reproducible. Data obtained from this experiment are plotted in Fig. 118.46, along with the prediction from Eq. (6). For rising voltage, the model predicts a column height h with reasonable accuracy; the discrepancies are almost certainly due to (1) uncertainties in the values for a and b, which must be measured before the fixture is cooled
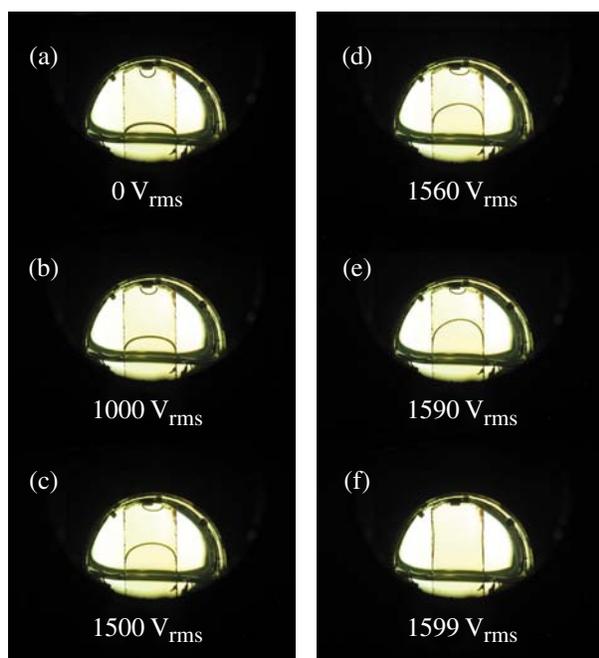
E18034JR

Figure 118.44
Meniscus of cryogenic D_2 at 23.9 K viewed through transparent, slightly convergent ITO-glass electrodes; $w = 7.6$ mm, $H = 12$ mm, $a = 0.42$ mm, $b = 1.41$ mm, for increasing ac voltages at 1 kHz. The small droplet visible at the top was trapped in a previous experiment. (a) $V = 0$ V_{rms}; (b) $V = 1000$ V_{rms}; (c) $V = 1500$ V_{rms}; (d) $V = 1560$ V_{rms}; (e) $V = 1590$ V_{rms}, meniscus approaching h^*; (f) $V = 1599$ V_{rms}, liquid has jumped to the top.
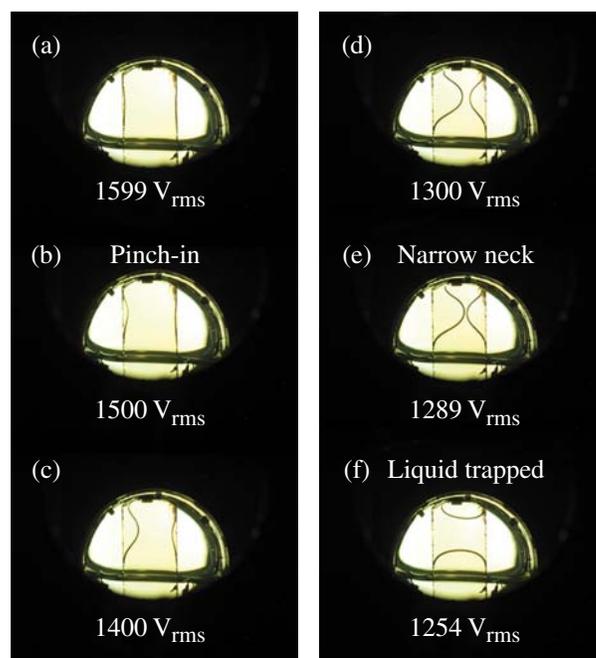
E18035JR

Figure 118.45
Meniscus of cryogenic D_2 at 23.9 K viewed through transparent, slightly convergent ITO-glass electrodes; $w = 7.6$ mm, $H = 12.0$ mm, $a = 0.42$ μm, $b = 1.41$ μm, for decreasing ac voltages at 1 kHz. (a) $V = 1599$ V_{rms}; (b) $V = 1500$ V_{rms}, surface starting to recede inward; (c) $V = 1400$ V_{rms}, further receded; (d) $V = 1300$ V_{rms}, further receded; (e) $V = 1289$ V_{rms}, only a narrow neck remains; (f) $V = 1254$ V_{rms}, neck has ruptured and liquid is trapped at the top.

Liquid jumps to top
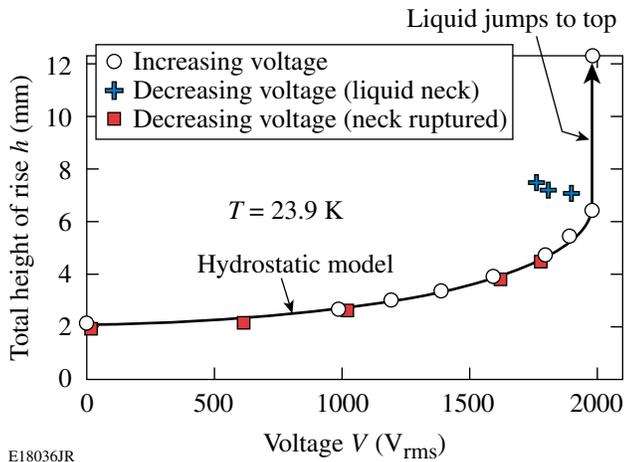
E18036JR

Figure 118.46
Experimental data and predicted $h(V)$ curve from Eq. (6) for converging plates, $w = 7.6$ mm, $H = 12$ mm, $a = 0.42$ μm, $b = 1.41$ μm. The data obtained for increasing voltage match the prediction very well. For decreasing voltage, data indicated by crosses (+) indicate the location along the vertical side where the interface is pinched in the most. The squares (■) denote the height of the column after the neck has ruptured.

down, and (2) a slight misalignment of the plates. A clear manifestation of this misalignment is the evident asymmetry of the meniscus profile that increases as voltage is raised. The data in Fig. 118.46 for reducing voltage are plotted in two groups: The crosses (+), indicating the locations of the narrowest point of the liquid neck shown in Figs. 118.45(b)–118.45(e), seem to correlate reasonably well with the calculated value of h^{*}. The squares (■), indicating measured column height values after the neck has ruptured, closely follow the cubic relation [Eq. (6)].

In the experiment shown in Figs. 118.44 and 118.45, the plates were maintained in position by a spacer positioned at the top–middle. This spacer has the effect of retaining some of the liquid at the top, even when the voltage is reduced to zero. Without this spacer, the trapped liquid always seems to fall. Such behavior is unlike the highly repeatable trapping phenomenon observed with room-temperature dielectrics,[18] where wetting hysteresis may help to hold the trapped liquid near the top when the voltage is removed.

Discussion

The bifurcation behavior of liquid D_2 differs from the prediction based on the 1-D model and also from experiments with room-temperature dielectric liquids, but only when the voltage is reduced toward V^* from values above it. The cause of this discrepancy seems to be the very low contact angle that cryogenic deuterium exhibits against the ITO glass–coated electrodes. In contrast, the contact angles for the dielectric liq-

uids used in earlier experiments conducted at room temperature were in the range of ~70° to ~90° (Ref. 18). When $\theta_c \approx 0°$, a thin, remarkably stable filament of liquid between two plates persists, probably because its concave inter-electrode profile makes it energetically favorable. Equation (6) fails to predict the observed behavior for lowering voltage because the existence (and stability) of such filaments is not accounted for in the 1-D hydrostatic model. The data in Fig. 118.46 do suggest that surface equilibrium starts to fail near $z = h^*$ as we would expect, irrespective of the formation of the filament.

One major question about the use of DEP in laser target fueling is not addressed here: namely, that the liquid fuel for laser targets will necessarily contain liquid tritium, which is highly radioactive. The energetic electrons (β particles) emitted by tritium add space charge to the liquid bulk, rendering the liquid effectively conductive, although probably not ohmic in nature. One hypothesis is that the small current detected to flow in liquid D_2 when an electric field is applied is actually due to very small but unavoidable levels of tritium contamination.[19,20] If there is sufficient tritium present, the mobile charges may make the liquid behave as an electrical conductor. In that case, the DEP mechanism will become inoperative; however, it could still be possible to actuate the liquid electrically by exploiting the electrowetting mechanism. To do so, it is necessary to coat the electrodes with a thin dielectric layer. Electrowetting has been intensively studied and demonstrated to be very effective in the transport and manipulation of many room-temperature liquids ranging from DI water to liquid mercury.[21] An investigation of the electrowetting behavior in liquid DT would be an interesting, if challenging, experimental undertaking.

Conclusion

A simple, 1-D hydrostatic model for the behavior of liquid deuterium between parallel plates under combined capillarity and liquid dielectrophoresis successfully predicts the height of rise as long as the plates are sufficiently wide compared to their spacing, i.e., $w/d \gtrsim 8$. The capillary and DEP effects are additive: $h = h_{cap} + h_{DEP}$. The actual 3-D meniscus shape is predicted with reasonable accuracy using the Surface Evolver tool, which seeks a numerical solution using finite elements and surface energy minimization. If the plates are made to converge toward the top, the hydrostatic equilibria include a bifurcation effect if the ratio of the electrode separation at the bottom and the top (b/a) is large enough. This bifurcation might be used to trap liquid; however, at present, the reproducibility of the trapped volume for liquid D_2 is not good because of the formation of a highly stable liquid filament, which forms because cryogenic deuterium perfectly wets the plates. Precise

metering of cryogenic liquids using the bifurcation effect may not be possible unless this phenomenon can be avoided.

Beyond its potential use in the fueling of small targets for laser fusion, other interesting applications for electric field–mediated cryo-microfluidics may be envisioned. One possibility is in the emerging field of cryo-preservation, i.e., the long-term storage of biological cells at low temperature to be later thawed and used in therapeutic treatments. The barrier to a practical technology of cryo-preservation is the shear number of samples that have to be preserved and the difficulties associated with proper freezing and thawing of cells without incurring damage.[22] The capability offered by liquid DEP to dispense, move, and manipulate small volumes of liquid nitrogen might prove very useful in this field. The properties of N_2 relevant to cryo-DEP—namely, dielectric constant $\kappa \approx 1.4$, surface tension $\gamma \approx 0.009$ Nt/m, and density $\rho \approx 0.8$ kg/m^3 at temperature $T = 77$ K—suggest that this liquid can be manipulated readily by combining dielectrophoretic microfluidics and temperature control.

Appendix: Temperature-Dependent Properties of Liquid D$_2$

For convenience, empirical relations for the temperature dependencies of the relevant liquid deuterium properties are provided below. SI units are used and the temperature T is in degrees Kelvin:

liquid mass density in kg/m^3 [curve fit based on Ref. 9, p. 62]:

$$\rho_1(T) = -0.005231\, T^3 + 0.3119\, T^2 - 8.225\, T + 252.9,$$

$$18.7\ \text{K} \leq T \leq 35\ \text{K} \tag{A1}$$

saturated vapor mass density in kg/m^3 [curve fit based on Ref. 9, p. 57]:

$$\rho_{\text{v}}(T) = 2.03 \times 10^{-7}$$
$$\times 10^{\left[0.5671\, T + 0.01508\, T^2 + 0.000156\, T^3 \right]}, \tag{A2}$$

$$18.7\ \text{K} < T < 35\ \text{K}$$

liquid-vapor surface tension in Nt/m [curve fit based on Ref. 9, p. 64]:

$$\gamma(T) = 1.759 \times 10^{-7}\, T^3 - 1.356 \times 10^{-5}\, T^2$$
$$+ 1.296 \times 10^{-4}\, T + 4.986 \times 10^{-3}, \tag{A3}$$

$$18.7\ \text{K} \leq T \leq 37\ \text{K}$$

liquid dielectric constant [curve fit based on data in Ref. 19]:

$$\kappa_1(T) = 1.361 - 0.00403\, T,$$

$$20\ \text{K} \leq T \leq 23\ \text{K} \tag{A4}$$

Cryogenic deuterium perfectly wets most solids, in other words, $\theta_c = 0°$ (Ref. 10). Known exceptions exist for liquid D$_2$ in contact with pure Cs and Rb.[23]

REFERENCES

1. P. W. McKenty, V. N. Goncharov, R. P. J. Town, S. Skupsky, R. Betti, and R. L. McCrory, Phys. Plasmas **8**, 2315 (2001).

2. T. J. B. Collins, J. A. Marozas, R. Betti, D. R. Harding, P. W. McKenty, P. B. Radha, S. Skupsky, V. N. Goncharov, J. P. Knauer, and R. L. McCrory, Phys. Plasmas **14**, 056308 (2007).

3. M. S. Tillack *et al.*, in *Proceedings of the 20th IEEE/NPSS Symposium on Fusion Energy* (IEEE, Piscataway, NJ, 2003), pp. 624–627.

4. J. D. Sethian *et al.*, Nucl. Fusion **43**, 1693 (2003).

5. D. R. Harding, T. B. Jones, Z. Bei, D. H. Edgell, and S. H. Chen, presented at the 18th Target Fabrication Meeting, Lake, Tahoe, CA, 11–15 May 2008.

6. D. R. Harding, T. C. Sangster, D. D. Meyerhofer, P. W. McKenty, L. D. Lund, L. Elasky, M. D. Wittman, W. Seka, S. J. Loucks, R. Janezic, T. H. Hinterman, D. H. Edgell, D. Jacobs-Perkins, and R. Q. Gram, Fusion Sci. Technol. **48**, 1299 (2005).

7. R. G. Fax, M. Hurwitz, and J. R. Melcher, J. Spacecr. Rockets **6**, 961 (1969).

8. Y. Suda *et al.*, Cryogenics **36**, 567 (1996).

9. P. C. Souers, *Hydrogen Properties for Fusion Energy* (University of California Press, Berkeley, 1986), Chap. 5.

10. R. J. Good and G. V. Ferry, in *Advances in Cryogenic Engineering*, edited by K. D. Timmerhaus (Plenum Press, New York, 1963), Vol. 8, pp. 306–310.

11. M. Dreyer, A. Delgado, and H. J. Rath, J. Colloid Interface Sci. **163**, 158 (1994).

12. H. Pellat, C.R. Hebd. Seances Acad. Sci. **123**, 691 (1896).

13. T. B. Jones Jr. and J. R. Melcher, Phys. Fluids **16**, 393 (1973).

14. T. B. Jones, Mech. Eng. **96**, 27 (1974).

15. T. B. Jones, M. P. Perry, and J. R. Melcher, Science **174**, 1232 (1971).

16. K. N. Mathes, Electro-Technol. **72**, 72 (1963).

17. K. Brakke, *The Surface Evolver*, ver. 2.30, Susquehanna University, Selinsgrove, PA, software available from http://www.susqu.edu/brakke/ evolver/evolver.html, 1 January 2008.

18. T. B. Jones, J. Appl. Phys. **45**, 1487 (1974).

19. W. L. Willis, Cryogenics **6**, 279 (1966).

20. P. C. Souers *et al.*, Cryogenics **20**, 247 (1980).

21. J. Lee and C.-J. Kim, J. Microelectromech. Syst. **9**, 171 (2000).

22. H. Zimmermann *et al.*, IEE Proc., Nanobiotechnol. **151**, 134 (2004).

23. D. Ross, P. Taborek, and J. E. Rutledge, Phys. Rev. B **58**, R4274 (1998).